**Submitted to the International Journal of Applied Ceramics Technology (ACT)
on 17 January 2009**

Development of an In-situ Surface Deformation and Temperature Measurement Technique for SOFC Button Cell

Huang Guo, Gulfam Iqbal, and Bruce S. Kang

West Virginia University, Mechanical and Aerospace Engineering Department
Morgantown, WV 26506-6106, USA

Abstract

A novel experimental technique is developed to measure in-situ surface deformation and temperature of solid oxide fuel cell (SOFC) anode surface along with the cell electrochemical performance. The experimental setup consists of a NexTech Probostat^{TM} SOFC button cell test apparatus integrated with Sagnac interferometric optical method and infrared sensor for in-situ surface deformation and temperature measurement, respectively. Button cell is fed with hydrogen or simulated coal syngas under SOFC operating condition. The surface deformation is measured over time to estimate the anode structural degradation. The cell surface transient temperature is also monitored with different applied current densities under hydrogen and simulated coal syngas. The experimental results are useful to validate and develop SOFC structural durability and electrochemical models.

Keywords: SOFC; In-situ surface deformation and temperature measurement

Introduction

Solid Oxide fuel cell (SOFC) is a device that electrochemically converts chemical energy into electrical energy and heat. Due to its high operating temperature, SOFC offers more fuel flexibility and tolerance for fuel contaminants compare to other types of fuel cells. Therefore, it is potentially an efficient technology to directly utilize coal syngas for next generation clean power generation. Long-term stability is an important requirement for the application of SOFC technology. The useful life of SOFC depends on cell material degradation which is caused by the aggressive operating conditions.

In addition to electrochemical performance, structural integrity of SOFC anode is also important for the successful long-term operation. Presently, Nickel yttria-stabilized zirconia (Ni-YSZ) is the choice for SOFCs anode material. Anode-supported SOFC depends on the anode layer as mechanical support for electrolyte and cathode [1]. However, several studies [2-4] indicate that it is susceptible to coal syngas contaminants, which requires further investigation. The anode layer is inherently susceptible to mechanical failure when subjected to moderate stresses [5]. Stresses in the anode material may arise from a number of reasons such as coefficient of thermal expansion mismatch, residual stresses, spatial or temporal temperature, and external mechanical loading. Past studies investigated thermal cyclic and thermal aging effects on Ni-YSZ/YSZ bilayers with the results showed modification of residual stresses and reduction of material strength [6, 7]. Lara-Curzio et al, [7] also concluded that Ni-YSZ showed propensity for creep deformation at 800°C. Anode could also be degraded upon redox cycles due to the dimensional and microstructure changes. These dimensional changes generate internal stresses in the anode

- Supported by the Basic Energy Sciences Division, U.S. Department of Energy, NETL (National Energy Technology Laboratory), WV State EPSCoR Office and the West Virginia University under Grant No. DE-FG02-06ER46299.

and other cell components and can cause structural degradation, loss of performance, or even complete loss of structure integrity [8].
Electrochemical impedance spectroscopy (EIS) and voltammetry are the most popular methods for studying SOFC electrochemical performance [9]. In-situ Raman spectroscopy and fourier transform infrared spectroscopy (FTIR) are utilized to identify molecular structure of SOFC electrode surface [10, 11]. However, these techniques focus on electrochemical reaction and are carried out at temperature lower than standard SOFC operating temperature. A surface profilometry technique has been employed to characterize curvature or cracking behavior in SOFC electrolyte layer [12] but it is not capable of in-situ measurement.
The objective of this research is to develop an enabling technology for in-situ surface deformation and temperature measurement on SOFC anode surface under service conditions. The experimental results are useful for the validation of SOFC electrochemical and structural models. The experimental setup developed in this research, is also utilized to estimate the material parameters for a SOFC anode material durability model [13, 14]. The model incorporates thermo-mechanical and fuel gas contaminants degradation mechanisms to prediction long-term structural integrity of SOFC anode.

Experimental Arrangement

A NexTech Probostat^{TM} button cell test apparatus was modified and integrated with a Sagnac interferometric optical setup [15, 16] and infrared (IR) thermometer. As shown in Figure 1, the optical setup consists of a 20 mW diode laser (wave length λ= 658 nm, laser spot size diameter = 2 mm), beam splitters, polarizer and beam directing mirrors. A long-distance microscope fitted with a CCD camera was used to record the fringe patterns corresponding to out-of-plane surface rotation and an IR thermometer (OMEGA OS 3707) was employed to measure the cell surface temperature on the same spot.

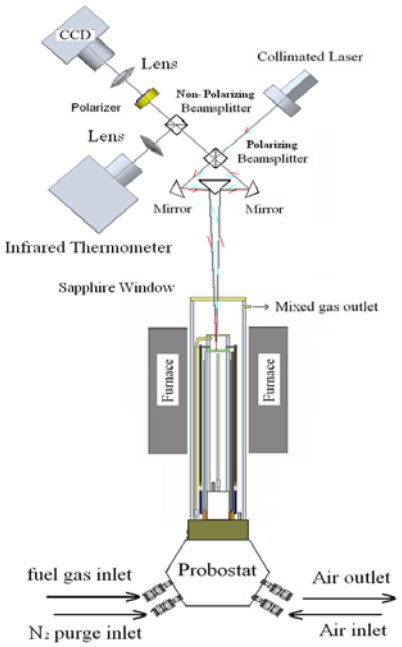

Figure 1. NexTech Probostate^{TM} integrated with Sagnac interferometry and IR thermometer

Anode-supported button cells, manufactured by MSRI (Materials and Systems Research Inc.), were tested in this study. Each button cell was about 2.6 cm in diameter with an anode composed of a 1 mm thick Ni-8YSZ support structure and a 25 μm thick interlayer of a highly catalytic Ni–8YSZ mixture. The electrolyte (8YSZ) was 20 μm thick and cathode was composed of a 25 μm thick $La_{0.8}Sr_{0.2}MnO_3$ (LSM)-8YSZ interlayer and a 25 μm thick current-collection layer of LSM. A nickel current collection mesh was attached to the anode using nickel contact paste. Similarly, a platinum mesh was attached to the cathode using platinum paste. Silver current cables and voltage taps were spot welded onto opposite sides of each current collection mesh. The button cell was mounted inside the Probostat™ using ARAMCO-516 high temperature cement. Alicat™ mass flow controllers (MFCs) were used to control fuel/air flow rates, pressure and fuel compositions. A temperature-controlled humidifier was used to control the water content of fuel gas supplied to the anode side.

Test Methodology

The button cell was heated from room temperature to 800°C over a time period of two hours. During this period, anode and cathode were supplied 100 sccm of N_2 and 250 sccm of air respectively. When the button cell reached its operating temperature, the fuel flow containing 10% H_2 and balanced with N_2 was provided for approximately two hours to reduce the anode and then switched to pure H_2 for another two hours. Once the reduction of anode was completed, the air flow was increased to 300 sccm.

To obtain fringe pattern and measure surface deformation of the button cell, a collimated laser light was split into two beams which travelled in identical but opposite directed paths as shown in Figure 1. The beams recombined to form stable interferometric fringe patterns which are related to the surface slope change but not to rigid body motion of the test specimen as schematically explained in Figure 2. The changes of the surface slope (S) and the corresponding out-of-plane displacements (W) can be represented by Eq. (1).

$$W = \frac{N \cdot \lambda}{2} \qquad (1)$$

where λ is the wavelength of the light source and N is the fringe order.

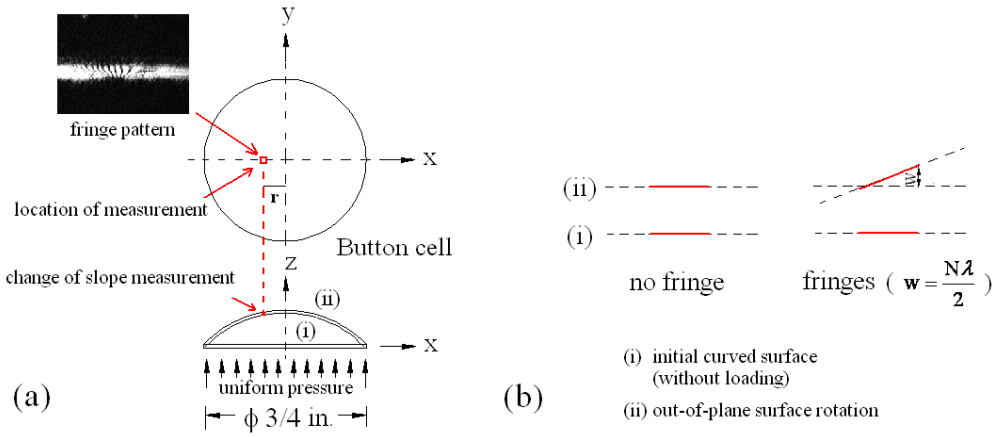

Figure 2. (a) Button cell under uniform pressure with corresponding fringe patterns on a spot location of the Ni wire mesh, (b) Button cell surface rotation before and after loading

After some trial runs, we found that the fringe patterns can be obtained on nickel wire mesh (current collector for anode) as shown in Figure 2(a). Notable advantages of this technique are: (i) the optical window does not affect/alter the fringe formation (ii) half wavelength measurement sensitivity (iii) immune to temperature fluctuation and (iv) immune to vibration, which make this optical technology suitable for in-situ non-contact measurement.

To establish connection between material degradation and the related experimental measurements, we modified a two-layer analytical solution [17] to obtain surface deformation Eq. (2), of a three-layered thin membrane under uniform pressure (Figure 3), which can be considered as a button cell with anode, electrolyte and cathode layers.

$$W = \frac{A_1}{A_1 \cdot C_1 - B_1^2} \cdot \frac{p \cdot r_o^4}{64} \left[1 - 2\left(\frac{r}{r_o}\right)^2 + \left(\frac{r}{r_o}\right)^4 \right] \qquad (2)$$

where r_o is the cell radius and

$$A_1 = \int_0^{ta} \frac{E_a}{1-\nu^2} dz + \int_{-te}^{0} \frac{E_e}{1-\nu^2} dz + \int_{-(te+tc)}^{-te} \frac{E_c}{1-\nu^2} dz$$

$$B_1 = \int_0^{ta} \frac{E_a}{1-\nu^2} z.dz + \int_{-te}^{0} \frac{E_e}{1-\nu^2} z.dz + \int_{-(te+tc)}^{-te} \frac{E_c}{1-\nu^2} z.dz$$

$$C_1 = \int_0^{ta} \frac{E_a}{1-\nu^2} z^2.dz + \int_{-te}^{0} \frac{E_e}{1-\nu^2} z^2.dz + \int_{-(te+tc)}^{-te} \frac{E_c}{1-\nu^2} z^2.dz$$

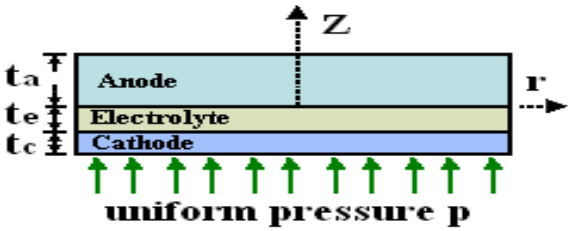

Figure 3. Button cell modeled as a three-layered thin membrane

The change of slope with the applied pressure (Eq. (3)) can be obtained by differentiating Eq. (2) with respect to the radius r.

$$\frac{\partial W}{\partial r} \Big/ p = \frac{A}{16}\left(r^3 - r \cdot r_o^2\right) \qquad (3)$$

where A is the combination of coefficients A_1, B_1, and C_1. Eq. (3) also provides the location of the maximum change of slope per unit applied pressure, which is at $1/\sqrt{3}$ of the normalized cell radius from the center. For this research, test results were conducted on this location.

For the actual experimental work, the button cell periphery is not tightly clamped and is relatively easy to rotate, similar to a simply supported circular plate. Thus a compensating factor is added to Eq. (3). By comparing the analytical solution of a clamped and simply supported single layer circular plate under uniform pressure [18], the slope of the simply supported plate can be deduced by multiplying the slope of the clamped plate with the following compensating factor C_o.

$$C_o = \left[(r/r_o)^2 - (3+\nu)/(1+\nu)\right]\left[1 - (r/r_o)^2\right]^{-1} \qquad (4)$$

For Poisson ratio of ν=0.3, the compensating factor C_o would be 3.31 at the location of maximum slope change ($r/r_o=1/\sqrt{3}$). From finite element analysis of the multi layered model (Figure 3), the compensating factor is determined to be in the range of 3.39 to 3.55. For the modeling purposes, we assume the compensating factor to be 3.5. Thu, Eq. (3) can now be written in the following form.

$$\frac{\partial W}{\partial r}\Big/ p = C_o \frac{A}{16}\left(r^3 - r.r_o^2\right) \qquad (5)$$

From the proposed experimental surface deformation measurement, anode material Young's modulus can then be determined from the three-layer model. Thus, a test methodology of long-time monitoring of SOFC anode structural integrity under simulated coal syngas operating condition can be carried out. Coupled with in-situ surface temperature and cell electrochemical measurements, correlation between the SOFC mechanical degradation and electrochemical degradation can be further studied.

Results and Discussion

In-situ Surface Deformation Measurements

The fringe patterns were obtained on Ni wire mesh located at 5.5mm from the center of the button cell. Preliminary work was carried out at room temperature (RT) with an in-house room temperature test apparatus and at 800°C using NexTech Probostat™ SOFC button cell test apparatus. The corresponding fringe patterns are shown in Figures 4 and 5, respectively.

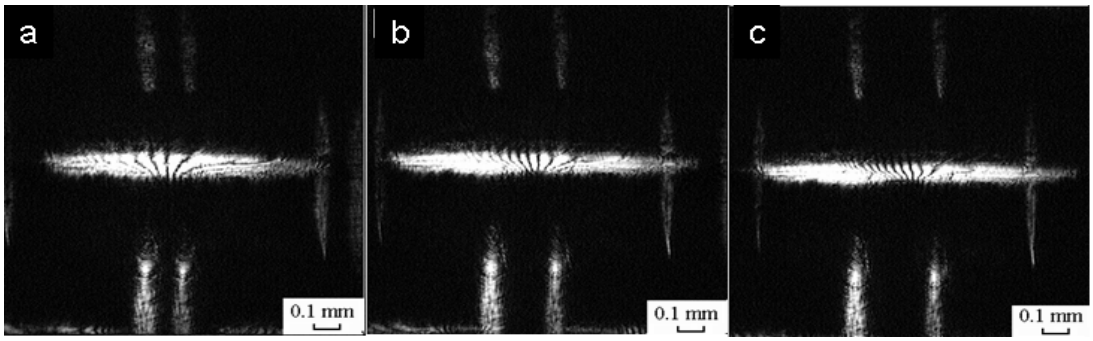

Figure 4. Fringe patterns on Ni mesh at RT with different applied pressures: (a) 0 kPa (0 psi), (b) 48.26 kPa (7 psi), and (c) 89.63 kPa (13 psi)

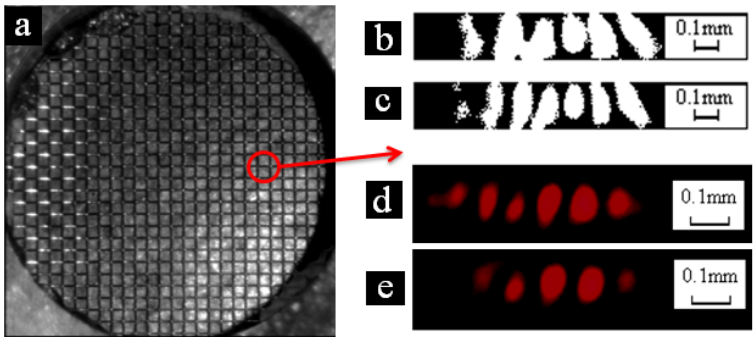

Figure 5. (a) Ni mesh and fringe patterns with different applied pressures: (b) 0 kPa (0 psi) (c) 131 kPa (19 psi) at RT, and (d) 34.47 kPa (5 psi) (e) 103.42 kPa (15 psi) at 800°C

As shown in Figures 4(a) and 5(b), the initial fringe patterns without applied pressure were due to the initial curved surface of the Ni wire. The fringe patterns changed as the applied air pressure on the cathode side is increased, as shown in Figures 4(b), 4(c), 5(c), 5(d) and 5(e).
The slope change per unit applied pressure was calculated for both the RT and 800^{o}C cases by counting the changes of fringe order versus applied pressure. The experimental results were compared with the finite element analysis and analytical solution and found to be in good agreement (within 5% error), as shown in Table1. These results support and validate the experimental methodology.

Table 1. Comparison among experimental, FE simulating and analytical results

Applied Pressure (kPa)		Experimental Results		Simulation Result	Analytical Result
		Slope S	ΔS/ΔP	ΔS/ΔP	ΔS/ΔP
Room temperature (RT)	34.47	4.038×10^{-3}	5.54×10^{-6}	5.37×10^{-6}	5.53×10^{-6}
	68.95	4.227×10^{-3}			
	103.42	4.420×10^{-3}			
800°C	34.47	5.484×10^{-3}	8.63×10^{-6}	9.17×10^{-6}	9.04×10^{-6}
	68.95	5.185×10^{-3}			
	103.42	4.889×10^{-3}			

Electrochemical performance

Once the cell was stabilized at its open circuit potential (OCV), I-V curve and EIS were measured using a Solartron electrochemical interface (SI 1287) and Solartron impedance analyzer (SI 1260). Figure 6 shows the power density history plot of the button cell during the cathode side air pressure changes for the surface deformation measurement. The cell was operating at 800^{o}C with 100 sccm H_2/3 vol.% H_2O and current density 0.5 A/cm^2. The cell performance was stable over time. However, it was affected significantly by the cathode side air supply interruption, as shown in Figures 6(b) and 6(c). The cell performance degraded immediately as the air flow decreased from 300 sccm to 100 sccm (point "1") and increased as the air outlet was closed (point "2"). It degrades again as the air inlet valve was closed at desired pressure (point "3") and recovered gradually when the air inlet valve was opened again to increase pressure (point "4"). On the basis of electrochemical polarization [19, 20], oxygen starvation to the cathode side can explain the abrupt cell performance degradation. This procedure was repeated for each pressure increment to measure surface deformation. After each measurement, both air outlet and inlet valves were opened again and air flow was resumed to 300 sccm. As shown in Figure 6(b), the cell performance quickly returned to about 70% of the initial value (point "5"). However, it took more than 24hrs to fully recover. Such phenomenon can also be seen by just turning on/off cathode side air supply, as shown in Figure 6 (c)

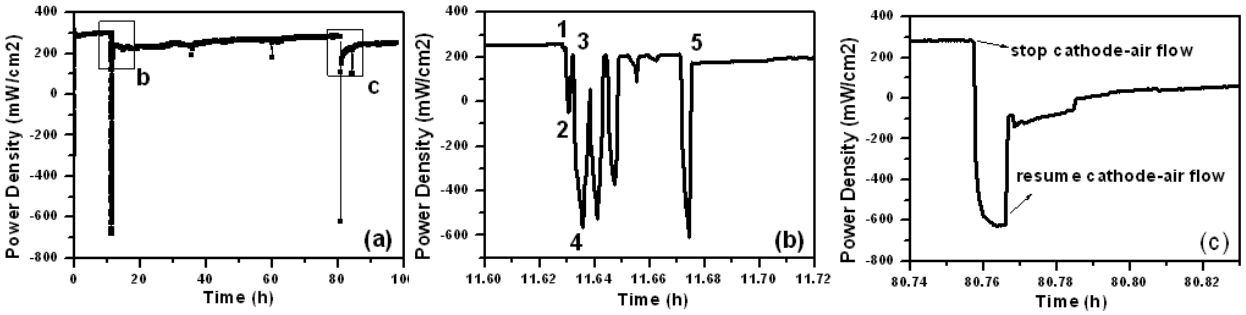

Figure 6 (a) Button cell power density plot during pressure changes (b) Effect of cathode side air pressure, (c) Effect of cathode side air flow rate

The I-V curves and the corresponding AC-impedance plots are shown in Figures 7 and 8, respectively. The impedance plot shows approximately the same charge-transfer resistance across the button cell with shifts of ohmic-resistance as found at the high-frequency x-intercept. After the cathode side air pressure interruption, the button cell showed an ohmic-resistance increase of 13%, while the button cell sustained performance loss, as shown in Figure 8. It also indicates that the power density of the button cell tended to recover over time due to the recovery of the cell's ohmic-resistance. To fix this problem discussed above, a remedial procedure was developed to minimize cathode-air interruption effect on SOFC performance. A pressure relief valve was installed to control cathode-air pressure that eliminates the need to cut off air supply and current supply was stopped when the cathode-air pressure is adjusted for the out-of-plane surface deformation measurement. The test data indicated that the pressure interruption problem is minimized through this procedure, as shown in Figure 9.

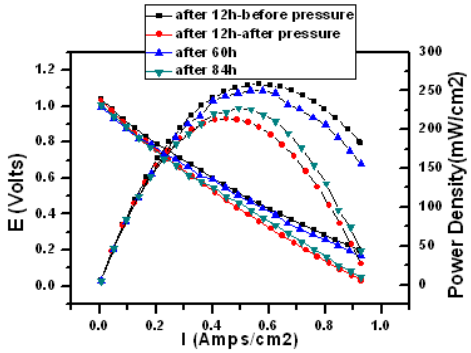

Figure 7. I-V curves of SOFC operating at 800 ^{o}C

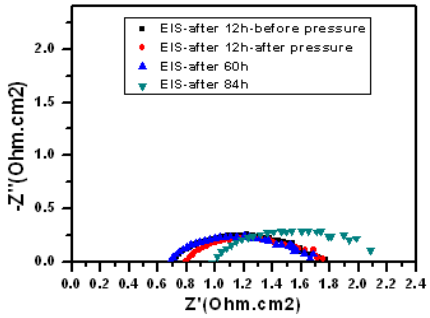

Figure 8. Impedance plots for SOFC operating at 800 ^{o}C, 0 V and 100 sccm H_2/3vol.% H_2O

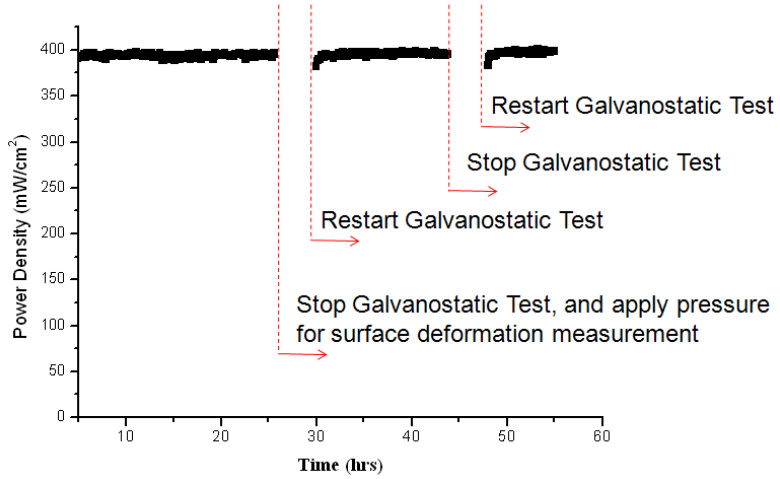

Figure 9.1 Remedy of cathode-air interruption on performance of SOFC with 100 sccm H_2/3vol.% H_2O at 800 ^oC (0.5 A/cm^2)

In-Situ IR Temperature Measurement

In general, accurate temperature measurement using IR thermometer depends on the field of view (FOV) which is defined as the distance-to-spot size ratio (D/S). OMEGA OS 3707 (D/S=60:1) gives approximately a 1 cm spot size at a distance of 60 cm. To get IR temperature measurement on a small spot area (~ 2 mm in diameter) of the button cell, Sagnac optical setup is utilized to allow some limited spectrum transmission (300 nm to 1000 nm) to the IR thermometer with a modified FOV. IR thermometer calibration was carried out with an embedded thermocouple close to the button cell. During heating of the cell, the data was recorded from IR thermometer and thermocouple simultaneously under steady test conditions. The thermal calibration data was linear as shown in Figure 10.

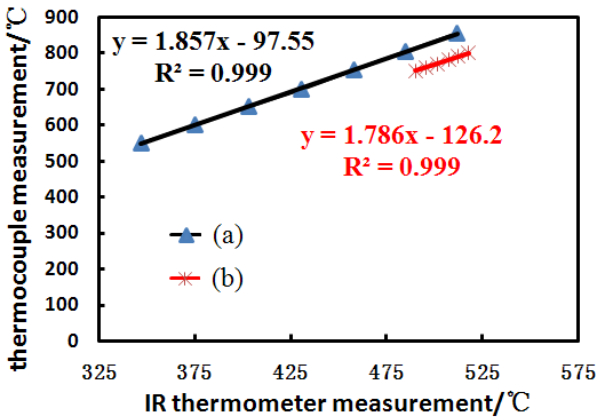

Figure 10. Steady-state IR temperatures calibration based on a thermocouple measurement under different environments: (a) air and (b) hydrogen.

It was observed that IR temperature calibrations were different for different testing conditions. Thus, on-line calibration is needed in order to get accurate temperature measurement. We have also conducted testing of in-situ surface IR temperature measurement as a function of loading current densities under H_2 environment as shown in Figure11, which shows that the cell temperature increases non-linearly with increased current density. The experimental data is useful to validate SOFC electrochemical models.

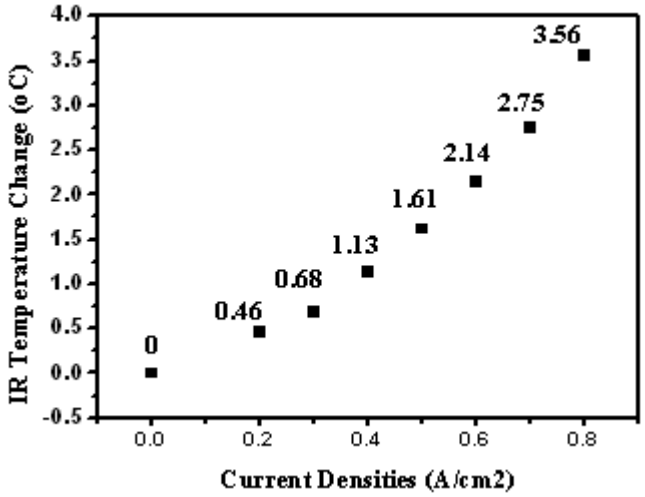

Figure 11. Steady-state surface temperature changes of button cell at different loading current densities with 100 sccm H_2/3 vol.% H_2O (Surface temperature T = 800.06 ^oC at i = 0 A/cm^2)

Conclusions

A novel experimental technique is developed to measure in-situ surface deformation and temperature on anode surface of a solid oxide fuel cell (SOFC) button cell, along with cell electrochemical performance measurement under operating conditions. A NexTech Probostat^{TM} SOFC button cell test apparatus was modified and integrated with Sagnac interferometric optical setup and IR thermometer. This optical technique is capable of in-situ, non-contact, electrode surface deformation and temperature measurement under SOFC operating conditions. The surface deformation measurement sensitivity is half wavelength and is immune to temperature fluctuation and environmental vibration. The experimental data is useful for validation and further development of SOFC structural and electrochemical modeling analyses.

Acknowledgement

Technical assistance from the research teams of Dr. I. Celik and Dr. Nick Wu of the WVU EPSCoR project team is very much appreciated.

References

[1] D. Larrain, J. Van herle and D. Favrat, “Simulation of SOFC Stack and Repeat Elements Including Interconnect Degradation and Anode Reoxidation Risk,” J. Power Sources., 161 392-403 (2006).

[2] O. Marina, L. Pederson, C. Coyle, EC Thomsen, D. Edwards, C Nguyen, G. Coffey, "Interactions of Ni/YSZ Anodes with Coal Gas Contaminants," Proceeding of the 9th Annual Solid State Energy Conversion Alliance (SECA) Workshop, Pittsburgh, PA, 2008.

[3] G. Krishnan, P. Jayaweera, J. Perez, "Effect of Coal Contaminants on Solid Oxide Fuel System Performance and Service Life," SRI Technical Progress Report 4 Quarter, 2006.

[4] O. Marina, L. Pederson, G. Coffey, C. Coyle, "Coal-based fuel cell technology: status, needs, and future applications," Mini Symposium, Morgantown WV, 2007.

[5] W. Li, K. Hasinska, M. Seabaugh, S. Swartz and J. Lannutti, "Curvature in Solid Oxide Fuel Cells", J. Power Sources., 138 145-155 (2004).

[6] K. Tsukuma, Y. Kubota, and T. Tsukidate, "Thermal and Mechanical Properties of Y_2O_3-Stabilized Tetragonal Zirconia Polycrystals", Advances in Ceramics, Vol. 12, Science and Technology of Zirconia II. Edited by A. H. Heuer and L. W. Hobbs. American Ceramic Society, Columbus, OH, 1984.

[7] E. Lara-Curzio, M. Radovic, R. M. Trejo, et al., "Reliability and Durability of Materials and Components for Solid Oxide Fuel Cells", Fuel Cell Program Annual Report, 82-89, (2005).

[8] D. Sarantaridis, and A. Atkinson, "Redox Cycling of Ni-Based Solid Oxide Fuel Cell Anodes: A Review," Fuel Cells, 07 [3] 246-258 (2007).

[9] A. Bieberle, L. P. Meier, ande L. J. Gauckler, "The Electrochemistry of Ni Pattern Anodes used as Solid Oxide Fuel Cell Model Electrodes", J. Electrochem. Soc. 148 A646-A656 (2001).

[10] M. B. Pomfret, J. C. Owrutsky, and R. A. Walker, "High-Temperature Raman Spectroscopy of Solid Oxide Fuel Cell Materials and Processes," J. Phys. Chem. B, 110[35] 17305-17308 (2006).

[11] X. Y. Lu, P. W. Faguy, and M. L. Liu, "In Situ Potertial-Dependent FTIR Emission Spectroscopy A Novel Probe for High Temperature Fuel Cell Interfaces," J. Electrochem. Soc. 149[10] A1293-A1298 (2002).

[12] W. X. Li, K. Hasinska, M. Seabaugh, et al., "Curvature in Solid Oxide Fuel Cells", J. Power Sources, 138, 145-155 (2004).

[13] G. Iqbal, H. Guo, and B. Kang, "Continuum Degradation Model for SOFCs Anode Material under Coal Syngas and its Implementation in FEA to predict Long-Term Structure Integrity," Proceeding of the Twenty-Fifth Annual International Pittsburgh Coal Conference, Pittsburgh, PA, September 29- October 2, 2008.

[14] G. Iqbal, H. Guo, and B. Kang, "Structural Degradation Mechanisms of SOFCs Anode and FEA for Long-Term Anode Material Behavior in Coal Syngas Environment," Proceeding of Material Science & Technology 2008, Pittsburg, PA, October 5-9, 2008.

[15] G. Sagnac, “L'ether lumineux demontre par l'effect du vent relatif dether dans un interferometre en rotation uniforme,” C. R. Acad. Sci., Paris 95 708-710 (1913).

[16] B.S. Kang and S.M. Anderson, “Experimental Investigation of 3-D Crack-Tip Deformation using Combined Moire-Sagnac Interferometry,” ASME J. of Pressure Vessel Technology., 123 124-129 (2001).

[17] J. H Nicholas et al, “Mechanics of Composite Structures,” MIT Press, (1969).

[18] S. P. Timoshenko and S. Woinowsky-Krieger, “Theory of Plates and Shells,” McGraw-Hill Book Company, Inc., New York, (1959).

[19] J. O. M. Bockris and S. Srinivasan, “Fuel Cells: Their Electrochemistry,” 176-229 McGraw-Hill Book Company, Inc., New York, 1969.

[20] R.H. Song, C.S. Kim, and D. R. Shin, “Effects of Flow Rate and Starvation of Reactant Gases on the Performance of Phosphoric Acid Fuel Cells”, J. Power Sources., 86 289-293 (2000).